Energy Conversion and Management 120 (2016) 257–273

Contents lists available at ScienceDirect

Energy Conversion and Management

journal homepage: www.elsevier.com/locate/enconman

Techno-economic assessment of membrane assisted fluidized bed reactors for pure H_2 production with CO_2 capture

V. Spallina [a,*], D. Pandolfo [b], A. Battistella [a], M.C. Romano [b], M. Van Sint Annaland [a], F. Gallucci [a]

[a] Chemical Process Intensification, Chemical Engineering and Chemistry Department, Eindhoven University of Technology, Eindhoven, The Netherlands
[b] Group of Energy Conversion Systems, Department of Energy, Politecnico di Milano, Milano, Italy

ARTICLE INFO

Article history:
Received 11 March 2016
Received in revised form 17 April 2016
Accepted 21 April 2016

Keywords:
H_2 production
Reforming
Membrane
Chemical looping
CO_2 capture

ABSTRACT

This paper addresses the techno-economic assessment of two membrane-based technologies for H_2 production from natural gas, fully integrated with CO_2 capture. In the first configuration, a fluidized bed membrane reactor (FBMR) is integrated in the H_2 plant: the natural gas reacts with steam in the catalytic bed and H_2 is simultaneously separated using Pd-based membranes, and the heat of reaction is provided to the system by feeding air as reactive sweep gas in part of the membranes and by burning part of the permeated H_2 (in order to avoid CO_2 emissions for heat supply). In the second system, named membrane assisted chemical looping reforming (MA-CLR), natural gas is converted in the fuel rector by reaction with steam and an oxygen carrier (chemical looping reforming), and the produced H_2 permeates through the membranes. The oxygen carrier is re-oxidized in a separate air reactor with air, which also provides the heat required for the endothermic reactions in the fuel reactor. The plants are optimized by varying the operating conditions of the reactors such as temperature, pressures (both at feed and permeate side), steam-to-carbon ratio and the heat recovery configuration. The plant design is carried out using Aspen Simulation, while the novel reactor concepts have been designed and their performance have been studied with a dedicated phenomenological model in Matlab. Both configurations have been designed and compared with reference technologies for H_2 production based on conventional fired tubular reforming (FTR) with and without CO_2 capture.

The results of the analysis show that both new concepts can achieve higher H_2 yields than conventional plants (12–20% higher). The high electricity consumptions of membrane-based plants are associated with the required low pressure at the retentate side. However, the low energy cost for the CO_2 separation and compression makes the overall reforming efficiency from 4% to 20% higher than conventional FTR with CO_2 scrubbing. FBMR and MA-CLR show better performance than FTR with CO_2 capture technology in terms of costs mainly because of lower associated CAPEX. The cost of H_2 production reduces from 0.28 €/Nm^3_{H2} to 0.22 €/Nm^3_{H2} (FBMR) and 0.19 €/Nm^3_{H2} (MA-CLR).

1. Introduction

With more than 600 billion Nm^3/year capacity installed worldwide, H_2 represents an important product for the chemical industry [1], while the H_2 demand is constantly increasing due to its potential use as automotive fuel [2]. Natural gas steam reforming is the established process for H_2 production [3]. Generally, H_2 production is carried out in a multi-tubular fixed bed reactor (fired tubular reformer-FTR) using an external furnace to provide the heat of reaction or in an auto-thermal reforming (ATR) system in which an oxidant (air or pure oxygen) is fed to the system [3–6]. The following equilibrium limited reactions of steam methane reforming (SMR, Eq. (1)), irreversible methane partial oxidation (POX, Eq. (2)) and water gas shift (WGS, Eq. (3)) play a role:

$$CH_4 + H_2O \rightleftarrows 3H_2 + CO \quad \Delta H_0^{298K} = 206.2\ \text{kJ/mol} \tag{1}$$

$$CH_4 + \frac{1}{2}O_2 \rightarrow 2H_2 + CO \quad \Delta H_0^{298K} = -38\ \text{kJ/mol} \tag{2}$$

$$CO + H_2O \rightleftarrows H_2 + CO_2 \quad \Delta H_0^{298K} = -41.2\ \text{kJ/mol} \tag{3}$$

Conventional steam reforming processes are based on several conversion and separation steps which include the feedstock pretreatment and sulfur compounds abatement, high temperature

* Corresponding author at: Chemical Process Intensification Group (SPI), Chemical Engineering and Chemistry, Eindhoven University of Technology, P.O. Box 513, 5612 AZ Eindhoven, The Netherlands.
E-mail address: v.spallina@tue.nl (V. Spallina).

http://dx.doi.org/10.1016/j.enconman.2016.04.073
0196-8904/

Nomenclature

AR	air reactor
ATR	auto-thermal reforming
BEC	Bare Erected Cost, *M€*
CA	chemical absorption
CCF	capital charge factor
CCR	carbon capture rate
CLC	chemical looping combustion
CLR	chemical looping reforming
COH	Cost of Hydrogen, $\frac{€}{Nm^3_{H_2}}$
$C_{O\&M}$	operating and maintenance costs, *M€*
E_{act}	activation energy, kJ mol^{-1}
FBMR	fluidized bed membrane reactor
FR	fuel reactor
FTR	fired tubular reforming
HEN	heat exchange network
HP-IP-LP	high-intermediate-low pressure
HRF	hydrogen recovery factor, –
HT-IT-LT	high-intermediate-low temperature
MA-CLR	membrane assisted chemical looping reforming
MDEA	methyl diethanolamine
MEA	monoethanolamine
NGCC	natural gas combined cycle
P_0	permeability, mol s^{-1} m^{-2} $Pa^{-0.74}$
POX	methane partial oxidation
PSA	pressure swing adsorption
SPECCA	specific primary energy consumption for CO_2 avoided $\frac{MJ_{th}}{kg_{CO_2}}$
SMR	steam methane reforming
TOC	total overnight cost, *M€*
WGS	water gas shift

reforming, water gas shift reactor(s) and final H_2 separation in a pressure swing adsorption (PSA) unit in order to reach a high H_2 purity of 99.999%. The conventional plants lead to large CO_2 emissions (about 380–420 kg_{CO2}/Nm^3_{H2}) to the atmosphere, associated to the combustion of the PSA-offgas and part of the fuel feedstock to provide the heat for the endothermic reactions.

When including CO_2 capture, different separation systems may be adopted for different emission sources. The first emission source is CO_2 in the syngas, which is typically separated by MDEA scrubbing, prior purification in the PSA-unit. Capturing this CO_2 leads to an overall CO_2 capture ratio of 60% as discussed in [7–10]. The second emission source is the stack of the FTR furnace. In order to capture the CO_2 from this source and achieve overall capture efficiencies higher than 85–90%, it is possible to either use part of the decarbonized hydrogen as fuel in the furnace [10] or include a post-combustion capture unit at the gas stack of the reformer by MEA absorption [11].

The increased number of units also increases the CAPEX of the H_2 production with CO_2 capture. In order to reduce the costs of the plant, membrane reactors have recently been proposed as a valid alternative for both small and large-scale applications [12–17]. The advantage of membrane reactors is the possibility to shift the equilibrium toward the products by continuously extracting the H_2 through perm-selective membranes. Natural gas to H_2 conversion and H_2 separation can thus be carried out in one single unit which can be operated at a lower temperature (typically between 450 °C and 600 °C). At the retentate side it is possible to obtain a CO_2–rich gas stream at pressurized conditions which can be easily separated and sent to long-term storage. Pd-based membranes have been amply studied in the last decades as the best candidate because of their very high H_2 permeability and extremely high perm-selectivity at intermediate temperatures (400–700 °C) [13,18–21]. Based on this technology, De Falco et al. [22] studied the use of multi-stage reforming and membrane separation to enhance the methane conversion at 650 °C. In this configuration, after the CO_2 separation from the retentate, part of the remaining gas (mostly H_2 and unconverted CO and CH_4) is used as fuel in a gas turbine to produce additional electricity for the plant. The exhaust gases leaving the expander are used to provide the heat of reaction for the reforming unit leading to an overall decrease in the energy consumption by 10%. An economic assessment and comparison of this plant has been discussed in Iaquaniello et al. [23], and about 30% of cost reduction compared to the conventional steam methane reforming plant was predicted. Manzolini et al. [24] presented a techno-economic analysis of a steam reforming membrane reactor operated at 600 °C and 10 bar, fully integrated in an advanced large scale combined cycle with CO_2 capture. 100% of carbon capture rate (CCR) was achieved by using an Air Separation Unit to produce pure O_2 for the complete retentate combustion and the resulting N_2 is used as sweep gas at the permeate side to enhance the hydrogen recovery factor (HRF). Depending on the thermodynamic and economic assumptions, the achieved CO_2 avoidance ranges from 38.9 €/ton_{CO2} to 44.5 €/ton_{CO2} (to be compared with 48.5 €/ton_{CO2} of the reference NGCC with post-combustion capture). Jordal et al. [25,26] have proposed a different plant configuration using two different membrane reactors based on Pd and microporous membranes integrated in a NGCC with CO_2 capture, reaching almost 48% of electric efficiency. Atsonios et al. integrate H_2 membrane reactor for enhanced WGS for power generation reaching 50.6% of net electric efficiency [27]. Finally, Chiesa et al. [28] presented different configurations with integration of O_2 and H_2 perovskite membranes for power production yielding an electric efficiency ranging from 45% to almost 50% and more than 87% of CO_2 avoided.

Among the several solutions already proposed for CO_2 capture, the chemical looping technology represents one of the most promising and efficient alternatives since CO_2 separation is inherently integrated in the fuel conversion step [29]. In CLC systems, a metal oxide (named oxygen carrier) is oxidized by reacting it with air and reduced by converting a fuel into CO_2/H_2O (chemical looping combustion, named CLC) or a syngas (chemical looping reforming, named CLR). CLR consists of two reactors operated at high pressure in which the oxygen carrier and catalyst are circulated to transfer the oxygen and heat for the reforming reaction from the air reactor to the fuel reactor. CLR has been proposed by Ortiz et al. [30,31] using Ni-based oxygen carriers because this oxygen carrier can also act as catalyst for the methane reforming reactions. Based on a simplified thermodynamic analysis, it has been found that a H_2 yield of 2.74 mol_{H2}/mol_{CH4} can be achieved with a NiO/CH_4 molar ratio equal to 1.18 to sustain the endothermic reactions at the fuel reactor [30]. Up to now no detailed thermodynamic analysis of the CLR plant has been presented. Due to differences in catalytic activity and oxygen transfer capacity, different oxygen carrier materials have been considered for the CLR process [32]. Finally, a different approach for steam methane reforming has been proposed by Ryden et al. [33], where the chem-

ical looping reactors act as combustion chambers to provide the heat of reaction to the reforming tubes which are immersed into the fuel reactor which converts the PSA-offgas into CO_2/H_2O in the fuel reactor.

The main objective of this paper is the thermodynamic analysis and optimization of two different membrane assisted reforming processes and the comparison from a techno-economic point of view with the benchmark technologies based on FTR plant with and without CO_2 capture. The two new processes are fully integrated with the other parts of the plant. Specifically, both H_2 plant configurations are optimized by varying the operating temperatures and pressures, steam-to-carbon ratio and other operating conditions. The design of the novel membrane reactor is carried out supported by a dedicated phenomenological model. The model is used for the reactor design and evaluation of its performance. For the selected configurations, an economic assessment is carried out and a sensitivity analysis on natural gas cost, reactor, oxygen carrier durability and membrane area costs is presented to provide an overview of the two technologies and their profitability in comparison with current technologies with and without CO_2 capture.

2. Plants description

2.1. Reference plants

A state-of-the-art fired tubular reforming plant (FTR) has been considered as benchmark technology reproducing the plant described in Martinez et al. [10]. In this plant (Fig. 1), natural gas is first pre-heated up to 365 °C to convert sulfur compounds to H_2S and saturate any olefins in a catalytic hydrogenation reactor over a Co-Mo based catalyst operating in the range of 290–370 °C. H_2S is then adsorbed over a bed of ZnO. NG is then mixed with H_2O to achieve a S/C ratio of 3.4 in the reformer. An adiabatic pre-reforming is carried out at 490 °C over a Ni-based catalyst (generally the pre-reforming is carried out in the temperature range of 300–525 °C), which removes the higher hydrocarbons that are present in the natural gas to prevent excessive coke depositions. The pre-reformed natural gas is pre-heated up to 620 °C and introduced in an externally heated fired tubular reformer where the gas mixture is converted into synthesis gas (syngas) at 890 °C in tubes filled with catalyst (generally Ni-based) where 80% of the CH_4 is converted into H_2/CO. The selection of the S/C for the reformer is based on industrial practices for the production of H2 via SMR [34–36] to avoid Ni-based catalyst de-activation [37]. For the present benchmark reforming process, a reforming pressure of 32.7 bar has been selected based on industrial applications. After reforming, the syngas is cooled down to 338 °C by producing HP-steam at 100 bar and 485 °C. Syngas cooling is generally carried out in two different heat exchangers. The first one is a shell and tube gas boiler in which steam is produced. In this heat exchanger, the temperature of the syngas is reduced avoiding excessive tube overheating, which may otherwise be damaged by crevice corrosion [38]. Saturated steam leaving the steam drum is superheated downstream the gas boiler in a shell and tube which is typically U-shape and baffle plates type heat exchangers [38].

The syngas is later fed to an adiabatic WGS reactor operated between 330 and 430 °C, where more than 70% of the CO in the syngas reacts with H_2O and is converted into CO_2 and H_2. HT-WGS is carried out in multiple reactors over a Fe-Cr based catalyst. For the reference plant without CO_2 capture a single-stage WGS suffices, since the unconverted CO is later used as fuel in the furnace. After cooling the shifted syngas to ambient temperature, the H_2-rich syngas is fed to a PSA (Pressure Swing Adsorption) unit, which consists of multiple adsorption beds, filled with molecular sieves and activated carbon. The H_2 is produced with a purity higher than 99.999% and the PSA-off gas is combusted in the reformer burner to supply the heat for the endothermic reactions. The heat for the steam reforming reaction is supplied burning the PSA-offgas and part of the NG with air in the furnace which is surrounding the catalytic bed. Waste heat recovery downstream of the furnace is carried out in convective banks in which the feed reformers pre-heating as well as steam production is carried out. These heat exchangers are typically hairpin type HE and the air combustion pre-heating takes place in tube bundle-type equipment [38]. The steam produced is then sent to a steam turbine to produce electricity. Part of the intermediate pressure (IP) steam is sent to process to meet the S/C ratio, while the remaining stream is expanded to 6 bar and delivered to the steam line of the refinery for thermal use. The thermal integration of the plant and the heat recovery from syngas cooler (orange[1]) and exhaust gases (green) are depicted in the cumulative grant curves in Fig. 1.

When integrating CO_2 capture technologies in the FTR plant new components as well as different operating conditions are required. The considered benchmark plant with CO_2 capture plant (and the related thermal integration) is depicted in Fig. 2. The reformate syngas is shifted in two-stages WGS to enhance both CO_2 and H_2 production: after the LT-WGS which is carried out at 213 °C using a Cu–Zn catalyst supported on Al_2O_3, the CO content is below 0.2% with an overall CO conversion in WGS section higher than 98%. The H_2–CO_2 rich mixture is cooled down to ambient temperature and H_2O is condensed, the CO_2 is separated from the H_2 by means of methyl-di-ethanol amine (MDEA) absorption. Here, the CO_2 scrubbing unit is based on a chemical absorption process, which involves reversible reactions between the CO_2 and the solvent to form weakly bonded compounds. The pure CO_2 is then released, compressed and sent to the pipeline for long term storage, while the regenerated solvent is fed back to the absorber. Solvent regeneration is undertaken in a desorber column operated below 180 °C, in which low pressure (LP) steam is used in the reboiler. MDEA has been selected as solvent considering the intermediate CO_2 partial pressure and the limited heat requirement for solvent regeneration.

Part of the impure H_2 from MDEA plant is used as fuel in the furnace, where it is burned with pre-heated air producing low CO_2 exhausts gases. The remaining part of the H_2 is sent to the PSA for final purification. Compared to the FTR without CO_2 capture, in this process a S/C ratio of 4 is used to enhance the NG-to-H_2 conversion and reduce the amount of unconverted species which are later burnt with the H_2 stream in the furnace.

2.2. Fluidized bed membrane reactor (FBMR)

The fluidized bed membrane reactor considered in this work has been proposed by Gallucci et al. [15] and several experimental and numerical works have been published on this concept [16,39,40]. The system (shown in Fig. 3) is based on a membrane reactor using Pd-based membranes, where the H_2 produced (#15) via the SMR/WGS reactions is separated at high purity and compressed after cooling down to ambient temperature (#18). Part of the H_2 permeates through other U-shaped membranes and reacts with air (#9) at the permeate side in order to supply the heat for the reforming reaction. The gases leaving this membrane (#10) are rich in O_2 and therefore they are used to burn some CO, H_2 and CH_4 from the cryogenic CO_2 purification unit (#7) and subsequently used to pre-heat the feed gases and produce part of the steam required for the process. At the retentate side the exiting

[1] For interpretation of color in Fig. 1, the reader is referred to the web version of this article.

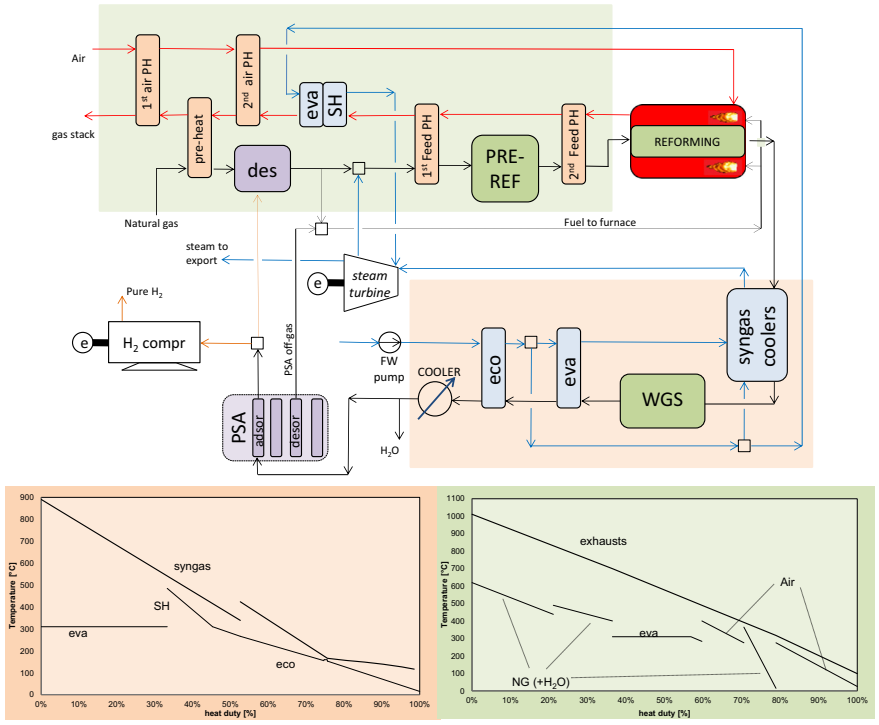

Fig. 1. Plant layout considered for the FTR plant without CO_2 separation and cumulative grant curves of the HENs.

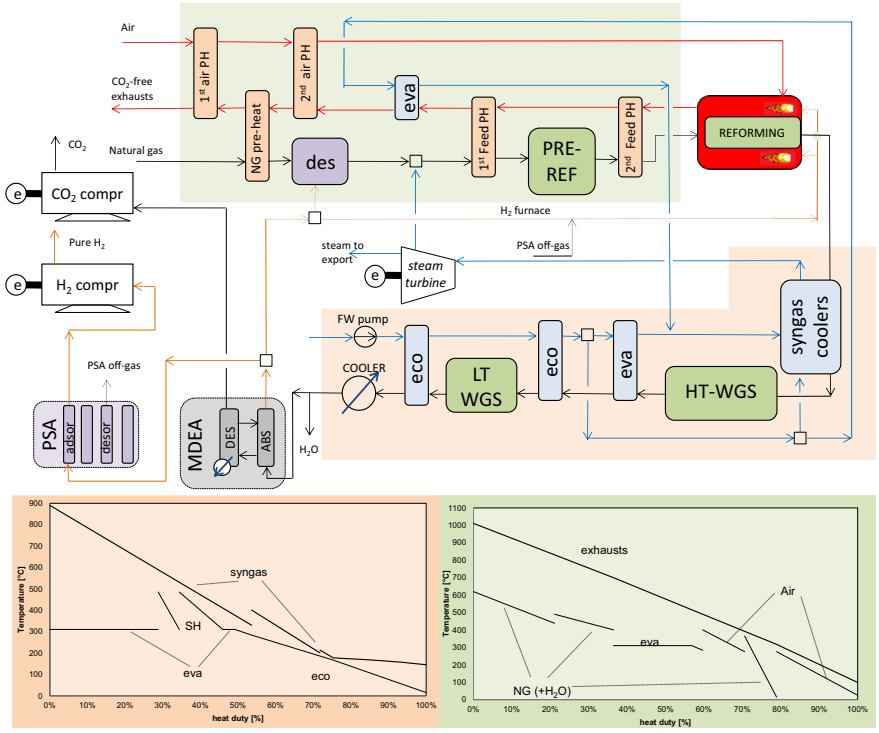

Fig. 2. Plant layout considered for the FTR plant with CA-MDEA for the separation of CO_2 and cumulative grant curves of the HENs.

gas (#4) mostly contains CO_2, H_2O and traces of H_2 and CO. Due to the high concentration and low volatility of the CO_2 compared to other components, a simplified CO_2 processing step based on low temperature phase separation can be used instead of a high energy demanding process based on physical and chemical absorption [41,42]. A two-flash auto-refrigerated cryogenic system has been designed according to Chiesa et al. [43]: after water condensation, the CO_2 rich stream is cooled down to −30 °C and part of the liquefied CO_2 is separated from the stream (#6) while the remaining gas is further cooled down in a second recuperative heat exchange below −53 °C to reach a deeper CO_2 recovery. The CO_2 is then throttled in order to supply the required cooling duty to the system

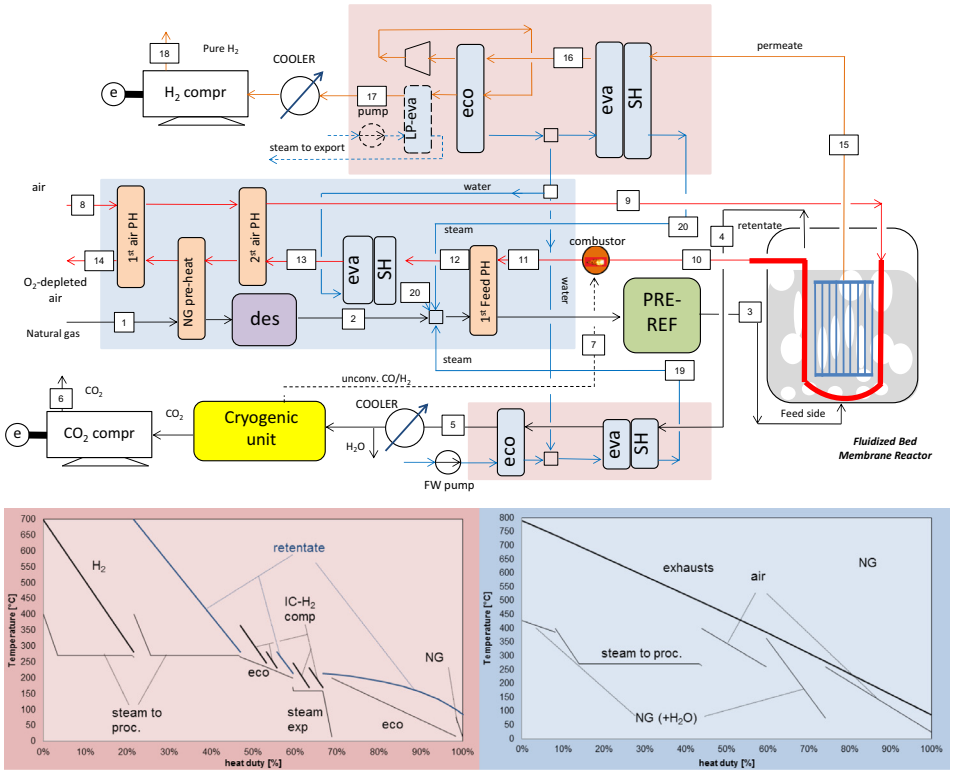

Fig. 3. Plant layout considered for the FMBR and cumulative grant curves of the HENs.

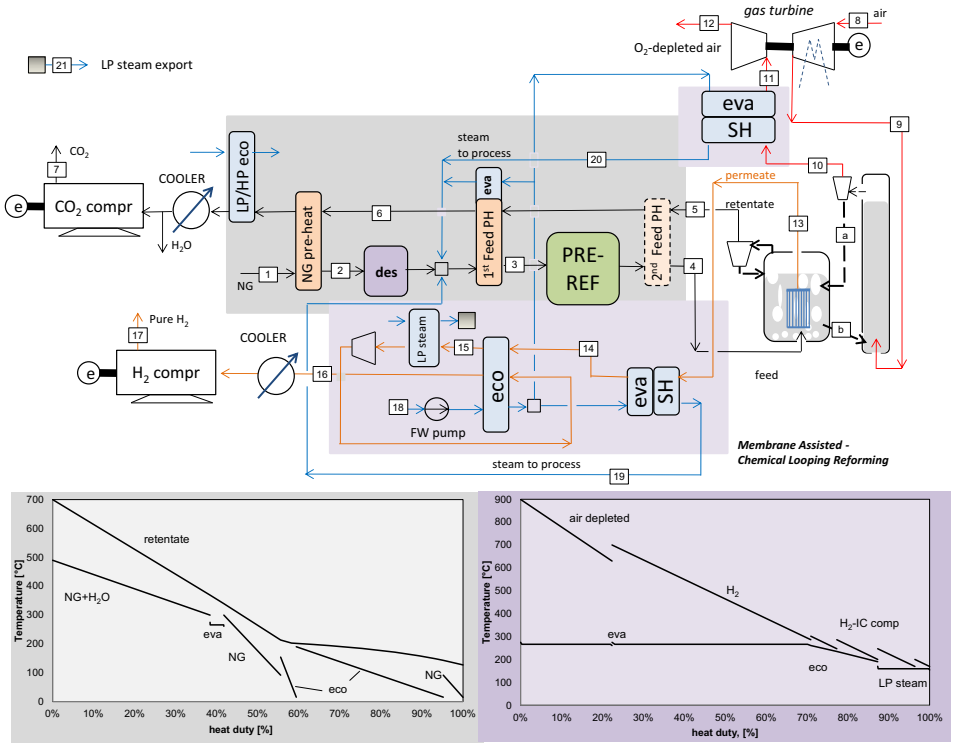

Fig. 4. Plant layout considered for the MA-CLR and cumulative grant curves of the HENs.

and after the recuperative heat exchangers is compressed to the final storage pressure. The vented gases are sent to the combustor after the membrane reactor. Due to the required S/C ratio, the total amount of steam produced from the gas cooling heat exchanger network has to be used for the process and therefore there is no steam cycle in this configuration however some steam is produced for the export depending on the operating conditions. This plant configuration can be also scaled-down to a smaller unit in which

the H_2 production plant can be integrated with other processes including also chemical processes using CO_2 as feedstock. Different process parameters have been varied to carry out the optimization of the process as discussed in later sections.

2.3. Membrane assisted chemical looping reforming (MA-CLR)

The membrane-assisted chemical looping reforming has been recently presented by Medrano et al. [44]. In this configuration, shown in Fig. 4, two reactors (named air reactor, AR and fuel reactor, FR) are used. In the FR, the fuel (stream #4) reacts with a metal oxide (NiO supported on $CaAl_2O_4$ [45]) to form H_2O and CO_2. Here, the Ni also acts as catalyst for the SMR and WGS reactions. The produced H_2 permeates through the membranes and therefore the CH_4 conversion is enhanced. Fresh NiO (#a) is fed from the top of the FR and therefore the unconverted fuel reacts with the oxygen carrier particles in the upper part of the reactor with two significant advantages: (i) at the reactor outlet it is possible to have a mixture of CO_2 and H_2O (#5) which does not require any downstream separation treatment and (ii) part of the NiO is reduced to Ni enhancing the catalytic properties of the solid material. The oxygen carrier also acts as heat carriers because it is introduced at higher temperature than the FR temperature (200 °C higher than in the fuel reactor). The oxygen carriers can also be de-activated in presence of low steam content. However, in case of chemical looping the solid circulation is also used to control the C formation since a high amount of O_2 is also available in the system as discussed by Cho et al. [46]. The H_2 from the permeate side (#13) is cooled down to ambient temperature and fed to the compressors before being delivered for final use (#17), while the retentate stream pre-heats the fuel and, after H_2O condensation, is compressed and sent for long term storage (#7). The CLR reactors operate high pressure (up to) 50 bar. The air reactor is fed with compressed air (#9) and the exiting O_2 depleted air is used first to produce the required steam for the process and then expanded before being released to the stack. An inter-cooled air compression is adopted to avoid too high temperatures at the compressor outlet which would require very expensive materials to withstand the severe conditions resulting from a pressure ratio of up to 50. Although from a thermodynamic point of view it may be more efficient to first expand the gas in the gas turbine and then recover the heat from the expanded air at the turbine outlet, in this work a different layout has been used because of the a lack of high temperature heat and an excess of low temperature heat available from other gases that makes this solution preferable from the thermodynamic and economic points of view.

2.4. Assumptions and methodology

In this section, the main assumptions related to both the thermodynamic assessment and the estimation of the costs of the plant are discussed. The main assumptions adopted are listed in Table 1. Most of the assumptions related to the heat exchangers, reactor conditions, CO_2 process unit for compression and purification as well as steam cycle and turbomachines efficiencies are taken from EBTF [47]. The FBMR has been modeled at chemical equilibrium for

Table 1
List of assumptions for the modeling of the plants and ranges considered for the selected variables in the sensitivity analysis.

Items	Plant configurations			
Raw material conditions	FTR	FTR + MDEA	FBMR	MA-CLR
CO_2 capture	NO	Amine-based	H_2 membrane + cryogenic	H_2 membrane
Natural gas	89% CH_4; 7% C_2H_6; 1% C_3H_8; 0.11% C_4H_{10}; 2% CO_2; 0.89% N_2 (70 bar and 15 °C)			
Air composition (vol.%)	77.3% N_2; 20.7% O_2, Ar 0.92%, H_2O 1%			
Process conditions				
Pre-reforming inlet temperature, °C	500	500	500	500
Reforming Temperature, °C	890	890	600–700 (uniform)	600–700 (uniform)
ΔT AR-FR, °C				200
Reforming pressure, bar	32.7	32.7	32–50	32–50
Steam-to-carbon ratio	2.7	4.0	2.5–3.5	1.5–2
Furnace temperature, °C	1010	1010	–	–
Pressure drops, % of inlet pressure	1	1	1	1
Heat exchangers				
ΔT_{min} gas–gas/gas–liquid	20/10	20/10	20/10	20/10
Pressure drops, % of inlet pressure	2	2	2	2
Air blowers				Not present
Hydraulic efficiency	0.8	0.8	0.8	
Mech-electric efficiency	0.94	0.94	0.94	
H_2 membrane	Not present	Not present		
Minimum p_{H2} difference, bar			0.2	0.2
Permeate pressure, bar			1–5	1–5
O_2 in the exhaust gases, vol.%			4%	
H_2 compressor and PSA				
PSA H_2 separation purity	89%	89%		
H_2 separation process, bar	29.7	29.7		
IC compression stages	3	3	Depending on the permeate pressure	Depending on the permeate pressure
Final H_2 conditions, T[°C]/p[bar]	30/150	30/150	30/150	30/150
H_2 outlet temperature, °C	30	30	30	30
CO_2 compression and purification	Assumptions from [47,43]			
Gas turbine	Not present	Not present	Not present	
Air compressor isentropic efficiency				92.5%
Gas expander isentropic efficiency				92.5%
Mech-electric efficiency				98%
Steam cycle parameters	Assumptions from [47]			
HP steam condition, T[°C]/p[bar]	485/92	485/92	–	–
HP steam pressure, bar	92	92	–	–
Steam export pressure, bar	6	6	6	6

Table 2
List of assumptions for the cost calculation of the plant components.

Equipment	Scaling parameter	Ref. capacity, S_0	Ref. erected cost, C_o (M€)	Scale factor, f	Cost year
Desulphurizer	Thermal plant input [MW_{LHV}]	413.8	0.66 [51]	0.67	2011
WGS reactors		1246.06	9.54 [11]	0.67	2007
Reformer + pre reformer reactors		1246.06	42.51 [11]	0.75	2007
Pre-reformer		1800	17.50 [52]	0.75	2005
PSA unit	Inlet flow rate [kmol/h]	17,069	27.96 [11]	0.6	2007
H_2 compressor	Power [HP]	1	0.0012 [53]	0.82	1987
Blower	Power [MW]	1	0.23 [52]	0.67	2006
Steam turbine	ST gross power [MW]	200	33.70 [51]	0.67	2007
Cooling systems	Heat rejected [MW]	13.19	17.18 [11]	0.67	2007
Amine-unit (MDEA)	CO_2 separated [kg/s]	68.2	46.14 [11]	0.8	2011
Cryogenic system	Duty [MW]	32	0.80 [54]	0.9	2013
CO_2 compressor	Power [MW]	13	9.9 [51]	0.67	2009
Reactor (FR, AR)	Vessel weight [lb]	130,000	7.32 [55]	0.6	2002
Cyclone	Inlet flow rate [m^3/s]	47.85	0.24 [55]	0.8	2013

a fixed minimum H_2 partial pressure difference between the retentate and the permeate side of 0.2 bar. In the FBMR, the amount of H_2 burnt in the U-shaped membranes is calculated to achieve auto-thermal operation and keep all the streams at the same outlet temperature. In the MA-CLR, the retentate gas at the end of the membrane is fully oxidized, as predicted by the reactor model discussed further on, resulting from a counter-current flow of the OC and the retentate gas within the reactor. The HRF is calculated in order to achieve auto-thermal operation and full conversion of the reactants at the retentate side. Thus, the minimum H_2 partial pressure difference across the membranes depends on the operating conditions. Complete reduction of the oxygen carrier is achieved in the fuel reactor, while the Ni to NiO conversion in the AR is not complete, but dictated by the amount of O_2 (air), which is the amount required to close the energy balance of the system. Therefore no O_2 is contained in the AR off-gases. The amount of air is varied to reach the desired operating temperature in the FR and the solids circulation rate is used to control the temperature difference between the AR and FR.

In order to define the component costs, several literature sources have been used as references (see Table 2). The cost of the syngas coolers have been calculated with Aspen Exchanger Design and Rating and compared with some data form manufacturers, the fluidized bed reactors cost has been calculated according to [48]. The gas turbine cost has been derived from [49]. Exponential scaling law has been used to calculate the equipment cost as function of scaling parameters, as indicated in Table 2. Each cost has later been adapted to the current equipment size and the cost actualized according to the chemical engineering cost index. The membrane specific cost is based on a Pall report [50] equal to 1000 \$/ft^2 (corresponding to 7900 €/m^2). The membrane lifetime is assumed to be 2 years [50].

2.5. Thermodynamic analysis

A schematic representation of the mass and energy balance of the four processes is depicted in Fig. 5. Each plant will convert the chemical energy from the natural gas into H_2, electricity and heat (as steam export) and will release to the environment part of the CO_2 while the remaining part will be captured and stored. Following the same approach from Martinez et al. [10] different indices have been chosen to determine the plant performance. In particular, in addition to standard hydrogen production efficiency and specific emissions (Eqs. (6) and (8)), equivalent efficiency and emissions are calculated (Eqs. (7) and (9)) based on equivalent natural gas input (Eq. (4)) and equivalent emissions (Eq. (8)) associated to electricity and steam import/export. In these way the calculation of performance takes into account the produced

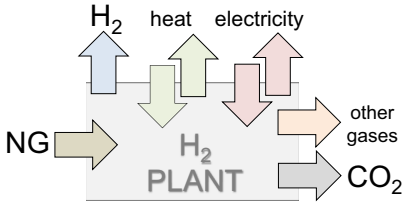

Fig. 5. Simplified mass/energy exchange of the considered systems.

H_2, the heat and the electricity production/demand as the same amount would be provided using state-of-the-art technologies as NGCC and industrial boiler represented by the η_{ref}. The same approach has been used for the calculation of the CO_2 emissions by using specific CO_2 emissions associated to the electricity and heat production from an external plant. The $SPECCA_{eq}$ (Eq. (10)) quantifies the energy cost in terms of primary energy to capture 1 kg of CO_2 and therefore takes into account both the energy penalization (to separate CO_2) and the reduced emissions with respect to a reference plant (in this case FTR without CO_2 capture).Finally the HR (Eq. (11)) is the typical efficiency (and units) used to quantifies the efficiency of an H_2 plant in the industry and therefore it has been also added in the comparison.

Equivalent natural gas flow rate

$$\dot{m}_{NG,eq} = \dot{m}_{NG} - \frac{Q_{th}}{\eta_{th,ref} \cdot LHV_{NG}} - \frac{W_{el}}{\eta_{el,ref} \cdot LHV_{NG}} \quad \text{where } \eta_{th,ref} = 0.9;\ \eta_{el,ref} = 0.583 \tag{4}$$

Steam export

$$Q_{th} = \dot{m}_{steam,export} \cdot (h_{steam@6bar} - h_{liqsat@6bar}) \tag{5}$$

H_2 production efficiency

$$\eta_{H_2} = \frac{\dot{m}_{H_2} \cdot LHV_{H_2}}{\dot{m}_{NG} \cdot LHV_{NG}} \tag{6}$$

equivalent H_2 production efficiency

$$\eta_{H_2,eq} = \frac{\dot{m}_{H_2} \cdot LHV_{H_2}}{\dot{m}_{NG,eq} \cdot LHV_{NG}} \tag{7}$$

CO_2 specific emissions (E_{CO2})

$$E_{CO_2} = \frac{\dot{m}_{CO_2,capt}}{\dot{m}_{NG} \cdot LHV_{NG} \cdot E_{NG}} \tag{8}$$

equivalent CO_2 specific emissions ($E_{CO2,\ eq}$)

$$E_{CO_2,eq} = \frac{\dot{m}_{CO_2,capt} - Q_{th} \cdot E_{th,ref} - W_{el} \cdot E_{el,ref}}{\dot{m}_{NG} \cdot LHV_{NG} \cdot E_{NG}} \quad \text{where } E_{th,ref} = 63.3\left[\frac{g_{CO_2}}{MJ_{th}}\right]; \quad E_{el,ref} = 97.7\left[\frac{g_{CO_2}}{MJ_{el}}\right] \tag{9}$$

Equivalent specific primary energy consumption for CO_2 avoided ($SPECCA_{eq}$)

$$SPECCA_{eq} = \frac{\frac{1}{\eta_{H_2,eq}} - \frac{1}{\eta_{H_2,eq,ref}}}{E_{CO_2,ref} - E_{CO_2,eq,ref}} \cdot 1000\left[\frac{MJ_{th}}{kg_{CO_2}}\right] \tag{10}$$

Energy consumption

$$HR_{tot} = \frac{\frac{\dot{m}_{NG} \cdot LHV_{NG} - Q_{th} - W_{el}}{4.186}}{\dot{N}_{H_2} \cdot 22.414}\left[\frac{Gcal_{NG}}{kNm^3_{H_2}}\right] \tag{11}$$

2.6. Economic analysis

The economic assessment has been carried out in order to compare the cost of H_2 following the methodology adopted from the global CCS institute [56]. The cost of H_2 is calculated as follows:

Cost of Hydrogen

$$COH = \frac{(TOC \cdot CCF) + C_{O\&M,fix} + (C_{O\&M,var} \cdot h_{eq})}{\dot{N}_{H_2} \cdot 22.414 \cdot 3600 \cdot h_{eq}}\left[\frac{€}{Nm^3_{H_2}}\right] \tag{12}$$

In which the TOC is the total overnight cost defined according to NETL [57] which includes any "overnight" capital expenses incurred during the capital expenditure period, except for the escalation and interest during construction (Table 3):

The TOC computes the COH using the capital charge rate factor (CCF) which defines a characteristic unit cost of the plant over the life of the plant accounting for all the expenditures that occur in different periods on a common value basis. Since the "first-year cost" methodology is applied, the rate for general inflation and real cost escalation are equal to zero. In order to determine the CCF different financial parameters have been used according to [11,47]. The resulting CCF for the entire plant equals 0.153. Operating and maintenance costs ($C_{O\&M}$) are divided in two parts: the fixed costs which account for the insurance, maintenance, labor wages, chemicals and membranes replacement, and the variable costs which are related to the cost of the fuel and water, as well as the revenue or cost associated with electricity production/ consumption and steam/heat export (Table 4). The plant availability is assumed equal to 90%.

Table 3
Methodology for the calculation of the TOC from NETL [57].

Plant component	Cost (M€)
Component W	A
Component X	B
Component Y	C
Component Z	D
Bare Erected Cost [BEC]	A + B + C + D
Direct costs as percentage of BEC	
Includes piping/valves, civil works, instrumentation, steel structure, erections, etc.	
Total Installation Cost [TIC]	80% BEC
Total Direct Plant Cost [TDPC]	BEC + TIC
Indirect costs [IC]	14% TDPC
Engineering procurement and construction [EPC]	TDCP + IC
Contingencies and owner's costs (C&OC)	
Contingency	10% EPC
Owner's cost	5% EPC
Total contingencies&OC [C&OC]	15% EPC
Total Overnight Cost [TOC]	EPC + C&OC

Table 4
Assumptions of the calculation of the O&M costs [24,54].

O&M-Fixed		
Labor costs	M€	1.5
Maintenance cost	% TOC	2.5
Insurance	% TOC	2.0
Catalyst and sorbent replacement		
Oxygen carrier cost [29]	$/kg	15
Reforming catalyst cost	k€/m^3	50
Water gas shift catalyst cost	k€/m^3	14
Desulphurization catalyst cost	$/ft^3	355
Lifetime	Years	5
Consumables		
Cooling water make-up cost	€/m^3	0.35
Process water cost	€/m^3	2
Natural gas cost	€/GJ$_{LHV}$	9.15
Miscellaneous		
Steam cost[a]	€/ton$_{steam}$	0.13
Electricity cost	(€/MW h)	76.36

[a] Based on the equivalent electricity to be produced.

3. Results

The results of the techno-economic analyses have been divided into three sections: in the first part, the optimization of the FBMR and MA-CLR plants is discussed. For the selected operating conditions, the reactor design is presented. Finally, the techno-economic assessment is discussed in the third part.

3.1. Thermodynamic optimization

The thermodynamic optimization focused on the most important operating conditions of the integrated membrane reactor. The membrane reactor operating temperature has been changed between 600 and 700 °C (assuming that in the near future stable high-flux membranes operating at 700 °C become available, while 600 °C should be considered as the maximum temperature for today's state-of-the-art high-flux membranes), the feed pressure has been varied from 32.5 bar to 50 bar and also the effects of the permeate pressure and steam-to-carbon ratio have been investigated.

3.2. FBMR

The results of the sensitivity analysis are summarized in Figs. 6 and 7. Referring to the plant configuration in Fig. 3, the following trends are highlighted:

- The η_{H2}, as well as the $\eta_{H2,eq}$, decreases by increasing the steam-to-carbon ratio because the amount of heat required for the steam generation, reduces the possibility to achieve a higher reactants pre-heating upstream of the membrane reactor and therefore more H_2 is required for the combustion membranes thus decreasing the net overall pure H_2 produced.
- Increasing the feed pressure increases the $\eta_{H2,eq}$: although the H_2 yield increases slightly (thereby changing the η_{H2}) a larger amount of steam for export is produced when the reactor works at higher pressure, because the steam is produced at higher pressure (and therefore the evaporator is working at higher temperature according to the saturation point). As consequence, more heat is available for the IT/LT heat recovery where the LP steam is produced.

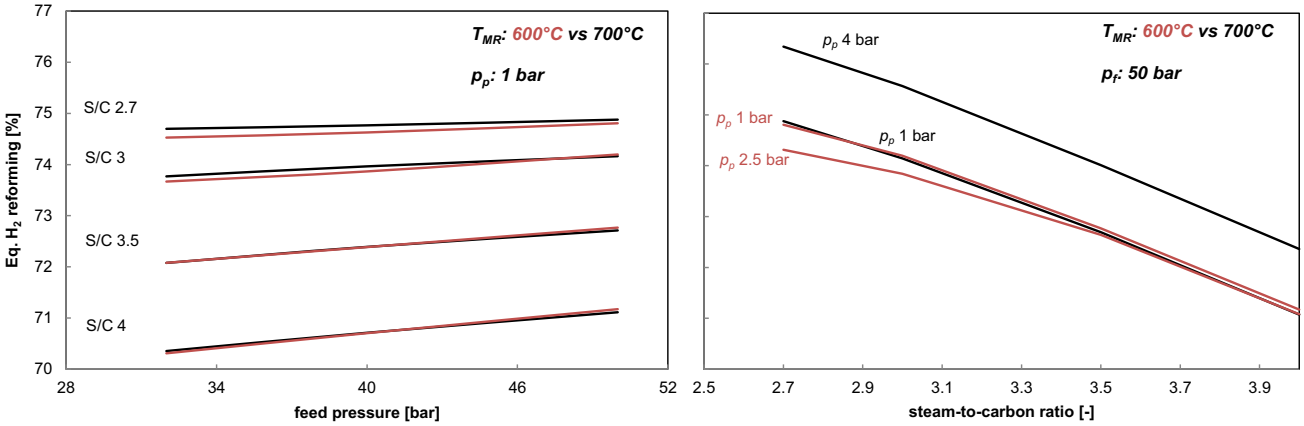

Fig. 6. Results of the FBMR sensitivity analysis for the equivalent H_2 efficiency.

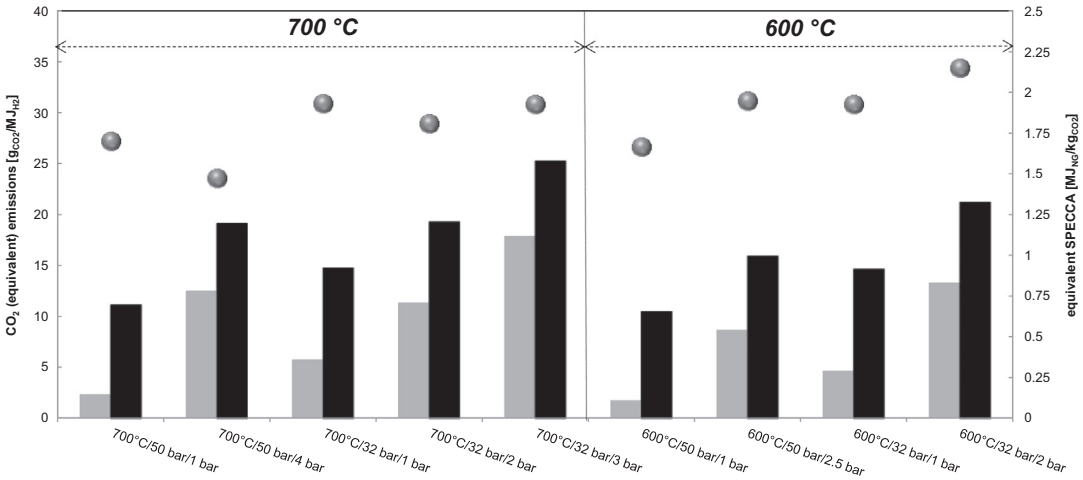

Fig. 7. Environmental performance of the FBMR in terms of CO_2 specific emissions (gray bars), equivalent CO_2 specific emissions (black bars) and SPECCA (points) as defined in the methodology section. Labels indicate temperature, feed pressure and permeate pressure.

– A lower reforming temperature slightly reduces the efficiency of the plant due to a small decrease in the CH_4 conversion.
– Increasing the permeate pressure (from 1 to 4 bar), at 700 °C leads to an increase in $\eta_{H2,eq}$, despite the decrease in η_{H2} due to the reduction of the H_2 yield by about 1%. The lower permeated H_2 flow causes an increase of the H_2 partial pressure at the retentate side and therefore a larger amount of H_2/CO is available at the cryogenic vent gas to pre-heat the reactants thus decreasing the amount of H_2 to be used for the combustion. On the other hand, the electricity consumption decreases by 23% due to the lower H_2 compression consumption and this effect dominates over the decrease in η_{H2}. A different trend is observed when the system is operated at 600 °C especially at lower S/C ratios, because the lower H_2 permeation and lower temperature cause a decrease in CH_4 conversion (0.2% vs 4% CH_4 vol. fraction at the retentate side by increasing the permeate pressure). Therefore, at this temperature the effect of a lower η_{H2} prevails over the decrease in electricity consumption.

In terms of CO_2 emissions, the CCR varies from 70% up to 95%, depending on the operating conditions. In general, the CO_2 emissions originate from the cryogenic vent gas which is burnt for heat recovery and released as stack gas: (i) at lower temperature, the amount of carbon containing compounds at the retentate side decreases because the lower CH_4 conversion is compensated for by a higher CO conversion into CO_2 which is subsequently separated, and therefore, at the cryogenic unit the overall CO_2 content in the exhaust gases decreases; (ii) the increase in the feed pressure and/or the decrease in the permeate pressure enhances the conversion to CO_2 at the retentate side due to the higher H_2 permeation and therefore the CO_2 emissions decrease. The $E_{CO2,eq}$ are higher than E_{CO2} because of the contribution associated with the electricity consumption. Overall, the $SPECCA_{eq}$ is slightly lower when working at 700 °C due to the $\eta_{H2,eq}$, in particular when the permeate side is at pressurized conditions (4 bar).

In Table 5, the thermodynamic conditions of the streams depicted in Fig. 4 are reported for the case at 700 °C, S/C of 2.7 and 50/4 bar at feed/permeate pressure.

3.3. MA-CLR

The fuel reactor is fed with pre-reformed syngas which reacts with the oxygen carrier to form reformate. The temperature difference between AR and FR is controlled by the solids circulation rate: the higher the solids circulation rate, the lower the temperature difference. As for the conventional ATR where the air/O_2 is varied in order to keep the system auto-thermal, in the CLR system the oxygen content (in terms of NiO) to the FR increases by increasing the air flow rate. For a high CH_4-to-H_2 conversion, a large amount of heat is required in the FR to sustain the reactions thermally. As

Table 5
Thermodynamic conditions of the selected streams represented in Fig. 3.

	T	p	m	N	MW	$N_i \times LHV_{i,mol}$		Composition (vol.%)								LHV	
#p	°C	bar	kg/s	kmol/s	kg/kmol	MJ	C_2^+	CH_4	CO	CO_2	H_2	H_2O	N_2	O_2	Ar	MJ/kg	MJ/kmol
1	15.0	70.0	2.62	0.15	18.02	121.9	As in the table of assumptions									46.5	837.5
2	365.0	70.0	2.62	0.15	18.02	121.9	8.11%	89.00%	0.00%	2.00%	0.00%	0.00%	0.89%	0.00%	0.00%	46.5	837.5
3	620.0	50.5	10.17	0.60	17.09	124.1	0.00%	23.70%	0.06%	2.78%	7.56%	65.69%	0.22%	0.00%	0.00%	12.2	208.5
4	700.0	49.5	9.07	0.32	28.10	15.8	0.00%	1.64%	5.33%	41.93%	8.49%	42.21%	0.40%	0.00%	0.00%	1.7	48.8
5	80.2	46.6	9.07	0.32	28.10	15.8	0.00%	1.64%	5.33%	41.93%	8.49%	42.21%	0.40%	0.00%	0.00%	1.7	48.8
6	30.0	110.0	5.52	0.13	43.10	1.9	0.00%	1.06%	1.66%	96.37%	0.78%	0.00%	0.13%	0.00%	0.00%	0.4	15.1
7	26.9	41.3	1.10	0.06	18.75	13.8	0.00%	6.72%	25.79%	20.44%	45.12%	0.00%	1.93%	0.00%	0.00%	12.6	236.3
8	24.8	1.1	15.63	0.54	28.86	0.0	0.00%	0.00%	0.00%	0.03%	0.00%	0.95%	77.35%	20.75%	0.92%	0.0	0.0
9	681.1	1.1	15.63	0.54	28.86	0.0	0.00%	0.00%	0.00%	0.03%	0.00%	0.95%	77.35%	20.75%	0.92%	0.0	0.0
10	700.0	0.9	15.87	0.60	26.42	0.0	0.00%	0.00%	0.00%	0.03%	0.00%	20.49%	69.76%	8.90%	0.83%	0.0	0.0
11	1225.4	0.9	16.97	0.64	26.58	0.0	0.00%	0.00%	0.00%	4.88%	0.00%	24.64%	65.81%	3.89%	0.78%	0.0	0.0
12	718.1	0.9	16.97	0.64	26.58	0.0	0.00%	0.00%	0.00%	4.88%	0.00%	24.64%	65.81%	3.89%	0.78%	0.0	0.0
13	112.7	1.0	16.97	0.64	26.58	0.0	0.00%	0.00%	0.00%	4.88%	0.00%	24.64%	65.81%	3.89%	0.78%	0.0	0.0
14	700.0	4.0	0.86	0.43	2.02	103.0	0.00%	0.00%	0.00%	0.00%	100%	0.00%	0.00%	0.00%	0.00%	120.0	242.0
15	281.0	4.0	0.86	0.43	2.02	103.0	0.00%	0.00%	0.00%	0.00%	100%	0.00%	0.00%	0.00%	0.00%	120.0	242.0
16	169.0	10.9	0.86	0.43	2.02	103.0	0.00%	0.00%	0.00%	0.00%	100%	0.00%	0.00%	0.00%	0.00%	120.0	242.0
17	30.0	150.0	0.85	0.42	2.02	102.3	0.00%	0.00%	0.00%	0.00%	100%	0.00%	0.00%	0.00%	0.00%	120.0	242.0
18	400.0	52.1	2.95	0.16	18.02	0.0	0.00%	0.00%	0.00%	0.00%	0.00%	100%	0.00%	0.00%	0.00%	0.0	0.0
19	400.0	52.1	2.61	0.14	18.02	0.0	0.00%	0.00%	0.00%	0.00%	0.00%	100%	0.00%	0.00%	0.00%	0.0	0.0
20	400.0	52.1	1.98	0.11	18.02	0.0	0.00%	0.00%	0.00%	0.00%	0.00%	100%	0.00%	0.00%	0.00%	0.0	0.0

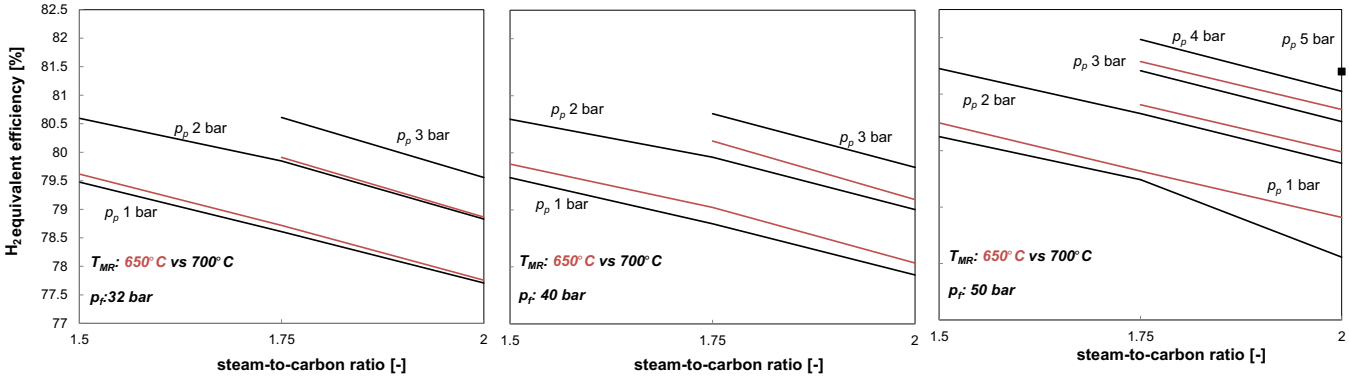

Fig. 8. Results of the MA-CLR sensitivity analysis at different conditions.

consequence, more air is fed to the AR to increase the Ni-to-NiO conversion and more fuel species (viz. H_2, CO and CH_4) react with NiO. When the reforming occurs with a high steam dilution, part of the heat supplied to the FR is required to increase the temperature of the H_2O excess to the reaction temperature and therefore more air is required to keep the system auto-thermal. Since the temperature difference between the AR and FR has been kept fixed (200 °C for all cases), the solids circulation rate changes in order to increase the heat transfer between the reactors. The results obtained from the MA-CLR optimization are shown in Fig. 8 and can be summarized with the following points:

- When increasing the S/C ratio the equivalent efficiency decreases because less hydrogen is produced: due to the higher amount of steam to the process, the syngas is fed to the FR at a lower temperature and therefore the amount of heat required at the FR increases (the amount of NiO converted in the fuel reactor slightly increases from 0.14 to 0.15 kmol/s), while the electric consumption and the heat generated as steam export remain substantially the same.
- At a higher reforming pressure (from 32 to 50 bar) the reforming efficiencies increases due to a reduced electric consumption (CO_2 is delivered at higher pressure).
- At a lower temperature (650 °C in this case), the overall efficiency increases: this is due to the reduced amount of heat from the reaction with oxygen carriers. Compared to the FBMR, the low S/C required enhances the performance at lower temperature because the heat available for gas cooling is sufficient to produce the steam for the process without compromising the reactants pre-heating.
- Increasing the pressure at the permeate side, the η_{H2} remains constant (the H_2 yield is the same), the steam to export does not change and the electricity consumption decreases due to the reduced H_2 compression consumption (e.g. at 50 bar and 700 °C about 16% less of the total power is required when increasing the p_{per} from 1 to 5 bar) resulting in an increase of $\eta_{H2,eq}$.
- The E_{CO2} are zero because the retentate gas is fully converted before leaving the reactor with the fresh oxygen carrier and therefore no carbon species are released to the atmosphere; therefore the equivalent CO_2 emissions are mainly associated to the electricity consumption.

In Table 6, the thermodynamic conditions of the streams depicted in Fig. 4 are reported for the case at 700 °C, S/C of 1.75 and 50/4 bar at feed/permeate pressure. The O_2-depleted air is cooled to 630 °C and after the expansion is released to the stack at 80 °C, while the heat from H_2 cooling is used exclusively for steam production (including LP steam). The release of gas to the ambient from the expander at temperature as low as 80 °C confirms the good process integration strategy deriving from high temperature heat recovery by steam generation, followed by gas expansion. Such high heat recovery efficiency would not be possible if heat recovery were performed after expansion of hot nitrogen stream exiting the air reactor, due to the lack of low temperature heat sink.

Based on the operating conditions of the membrane reactor, a phenomenological model [58] has been used in order to design the reactor and calculate the number of membranes and amount of oxygen carrier/catalyst required for the plant considered as detailed in the next section.

3.4. Reactor design

The membrane reactor design has been carried out using a one-dimensional two-phase phenomenological fluidized bed reactor model for the freely bubbling fluidization regime at steady state conditions. The model considers the gas moving upward through an emulsion and a bubble phase. The solids in the bubble wake move upward with the bubble and this flow is balanced by the downward motion of the solids in the emulsion phase. The system is assumed to be operated in the freely bubbling fluidization regime with a u/u_{mf} ratio in the range of 5–12 with the exception for some zones of the bed where the u/u_{mf} drops to 1.5 due to H_2 extraction. The membranes inside the reactor act as internals for the system and therefore the bubble diameter is limited enhancing in this way the mass transfer between bubble and emulsion phase. All the constitutive equations related to the hydrodynamics and mass transfer have been taken from Kunii–Levenspiel [59–61] and adapted as proposed by Iliuta [62]. Note that the correlations for the mass transfer have been derived for low pressure operation, which may considered as a worst case, since the mass transfer is expected to be improved when operating at higher pressures. The kinetics of the gas–solid and heterogeneous reactions have been selected according to some experimental data on the oxygen carrier characterization undertaken at Eindhoven University of Technology (TU/e) [45]. The permeation law has been derived from permeation tests that have been carried out on cylindrical high-flux Pd-based membranes using a metallic support [63,64]. The resulting H_2 permeation expression is given by:

Permeated H_2, mol/s

$$\dot{N}_{H_2}\left[\frac{mol}{s}\right] = \frac{P_0}{t_m}\exp\left(\frac{-E_{act,p}}{RT}\right)\cdot A_{mem}\left(p_{H_2,ret}^{0.74} - p_{H_2,perm}^{0.74}\right)$$

$$\text{where } P_0\left[\frac{mol}{s\,m\,Pa^{0.74}}\right] = 4.24\times10^{-4};\quad E_{act,p}\left[\frac{kJ}{mol}\right] = 5.81;\quad t_m = 5\,\mu m \tag{13}$$

Table 6
Thermodynamic conditions of the selected streams represented in Fig. 3.

	T	*p*	*m*	N	MW	$N_i \times LHV_{i,mol}$		Composition (vol.%)								LHV	
#p	°C	bar	kg/s	kmol/s	kg/kmol	MJ	C_2^+	CH_4	CO	CO_2	H_2	H_2O	N_2	O_2	Ar	MJ/kg	MJ/kmol
1	15	75	2.62	0.15	18.02	121.9	as in the table of assumptions									46.5	837.5
2	324	75	2.62	0.15	18.02	121.9	8.90%	89.00%	0.00%	2.00%	0.00%	0.00%	0.90%	0.00%	0.00%	46.5	837.5
3	490	51	7.52	0.42	17.9	121.9	2.80%	30.90%	0.00%	0.70%	0.70%	64.60%	0.30%	0.00%	0.00%	16.2	290.3
4	454.2	50.5	7.52	0.44	17.18	123.8	0.00%	33.40%	0.00%	2.70%	5.60%	58.00%	0.30%	0.00%	0.00%	16.4	281.4
5	699.9	49.5	9.01	0.27	33.41	0.3	0.00%	0.00%	0.20%	57.80%	0.20%	41.40%	0.50%	0.00%	0.00%	0.0	1.1
6	339.3	49.5	9.01	0.27	33.41	0.3	0.00%	0.00%	0.20%	57.80%	0.20%	41.40%	0.50%	0.00%	0.00%	0.0	1.1
7	30	110	6.98	0.16	43.71	0.3	0.00%	0.00%	0.30%	98.60%	0.30%	0.00%	0.80%	0.00%	0.00%	0.0	1.6
8	15	1	10.49	0.36	28.86	0.0	0.00%	0.00%	0.00%	0.00%	0.00%	1.00%	77.40%	20.80%	0.90%	0.0	0.0
9	503	50	10.49	0.36	28.86	0.0	0.00%	0.00%	0.00%	0.00%	0.00%	1.00%	77.40%	20.80%	0.90%	0.0	0.0
10	900	49.5	8.08	0.29	28.04	0.0	0.00%	0.00%	0.00%	0.00%	0.00%	1.20%	97.60%	0.00%	1.20%	0.0	0.0
11	630	49.5	8.08	0.29	28.04	0.0	0.00%	0.00%	0.00%	0.00%	0.00%	1.20%	97.60%	0.00%	1.20%	0.0	0.0
12	80.7	1	8.08	0.29	28.04	0.0	0.00%	0.00%	0.00%	0.00%	0.00%	1.20%	97.60%	0.00%	1.20%	0.0	0.0
13	700	4	0.92	0.46	2.02	111.3	0.00%	0.00%	0.00%	0.00%	100%	0.00%	0.00%	0.00%	0.00%	119.8	242.0
14	286	4	0.92	0.46	2.02	111.3	0.00%	0.00%	0.00%	0.00%	100%	0.00%	0.00%	0.00%	0.00%	119.8	242.0
15	200	4	0.92	0.46	2.02	111.3	0.00%	0.00%	0.00%	0.00%	100%	0.00%	0.00%	0.00%	0.00%	119.8	242.0
16	169	8.3	0.92	0.46	2.02	111.3	0.00%	0.00%	0.00%	0.00%	100%	0.00%	0.00%	0.00%	0.00%	119.8	242.0
17	30	150	0.92	0.45	2.02	108.9	0.00%	0.00%	0.00%	0.00%	100%	0.00%	0.00%	0.00%	0.00%	119.8	242.0
18	15	1	4.89	0.27	18.02	0.0	0.00%	0.00%	0.00%	0.00%	0.00%	100%	0.00%	0.00%	0.00%	0.0	0.0
19	275	52	3.2	0.18	18.02	0.0	0.00%	0.00%	0.00%	0.00%	0.00%	100%	0.00%	0.00%	0.00%	0.0	0.0
20	275	52	1.47	0.08	18.02	0.0	0.00%	0.00%	0.00%	0.00%	0.00%	100%	0.00%	0.00%	0.00%	0.0	0.0
21	170	6	0.66	0.04	18.02	0.0	0.00%	0.00%	0.00%	0.00%	0.00%	100%	0.00%	0.00%	0.00%	0.0	0.0
a	900	50	132.66	1.04	0	0.0		Ni 6.4%; NiO 14.5%, $MgAl_2O_4$ 79.1%									
b	700	50	130.25	1.04	0	0.0		Ni 21%, $MgAl_2O_4$ 79%									

For the FBMR the reactor design is carried out by changing the reactor geometry (diameter D_r and length L_r) and the membrane area - as a combination of membrane length (L_m), membrane diameter (d_m) and number of membranes (N_m) in order to achieve the same H_2 yield and retentate composition as from the Aspen simulation.

For the MA-CLR, the AR and the FR are operated simultaneously. The AR is designed by changing the reactor length and diameter to achieve the required solids conversion, while the FR design is carried out by varying different parameters: the number, length of the membranes have been varied to obtain the same H_2 flow permeated as in the thermodynamic analysis above discussed, while the reactor geometry is changed to obtain complete NiO reduction, and complete combustion of the fuel species at the retentate side. The energy balance of the system is not implemented in the reactor model, therefore, the presence of a temperature profile along the reactor could change the results. However, due to the high internal solids circulation, the temperature profile is expected to be virtually homogeneous for this system.

Based on the reactor design, the cost has been estimated (respectively for the reactor, membranes and particles) and a cost sensitivity analysis has been carried out in the next part of the paper, accounting also for the uncertainties associated to the cost estimation of the membrane reactor. The preliminary results of the simulations are shown in Fig. 9. It is possible to notice that: (i) for both cases, the CH_4 is converted along the entire reactor until it reaches the exit of the reactor; (ii) some influence of bubble-to-emulsion phase mass transfer limitation is evident from the differences of the concentration profiles for the emulsion and bubble phases; (iii) the presence of the membranes reduced the bubble size acting as internals in the reactor, with the advantage that the composition at the emulsion and bubble phases is not very different; (iv) for the MA-CLR the H_2 is produced at the beginning and the H_2 mol fraction decreases continuously until 10.2 m and after that the H_2, the CO and CH_4 are completely consumed because they react with NiO that is present at high concentration in the upper part of the reactor; (v) in the MA-CLR, the permeated H_2 increases from the beginning of the reactor and remains constant after 10.2 m which corresponds to the end of the membrane which leads to a strong gradient in the gas composition as shown in Fig. 9b) while in the FBMR the permeated H_2 increases until the end of the reactors; (vi) about 21% of the permeated H_2 in the FBMR reacts with air in the U-shaped membranes and therefore the number of membranes used for H_2 separation and combustion are respectively 109 and 8 (taking into account the different H_2 partial pressures at the retentate side). Based on the geometry calculated from the model, the cost of the reactor has been calculated as described in the next part.

The reactor costs have been defined by considering them as pressure vessels and the reference value used for the calculation is the one of a fluidized catalytic cracker (FCC) defined by NREL report [55]. The scaling factor assumed is the weight of the vessel. The starting point to calculate the size of the fuel reactors, are the reactor diameter and length obtained from the model simulations: following the procedure described in [65] it is possible to define the volume and consequently the total weight. The air reactor, which is usually considered as a riser is divided in two parts: a mixing zone that behaves as a bubbling fluidized bed, and a riser where the solids are transported upwards in order to be recirculated. Considering the superficial velocity of 1.2 m/s and the volumetric flow rate resulting from the mass balance, the sections of the reactor can be determined, and thus the diameter. For the mixing zone a ratio of 1.5 between length and diameter has been used, whereas for the riser the length has been assumed equal to 10 m. After having defined these values, it is possible to follow the same procedure described in [65] to calculate the weight of the air reactor.

3.5. Techno-economic evaluation

The energy balance and performance indices are shown for the selected cases in Table 7. Compared to the SMR plant without CO_2 capture, the conventional reformers with CO_2 capture with chemical absorption show a decay of more than 14 percentage point in $\eta_{H2,eq}$, because the heat required in the reformer is higher (due to the higher S/C), the electricity consumption is higher due to CO_2 compression and the steam export is significantly lower due to the steam required for the MDEA reboiler. The FBMR shows a higher η_{H2}, mostly because the temperatures of the gases are kept at relatively low temperature (around 700 °C) and therefore more input heat (as NG_{LHV}) is converted into H_2 heating value instead of sensible heat of the outlet gas streams. Due to the high reforming pressure, the CO_2 is available at high pressure and therefore the CO_2 compressor energy demand drops in comparison to the conventional system. On the other hand, H_2 is separated at a relatively low pressure (4 bar for the selected case) and therefore the electricity requited for the H_2 compression increases significantly. As explained before, the CO_2 emissions (both E_{CO2} and $E_{CO2,eq}$) are higher than for SMR with CO_2 capture because of the lower CO_2 capture efficiency of the cryogenic unit. In order to increase the CO_2 capture ratio, a WGS reactor can be added downstream of

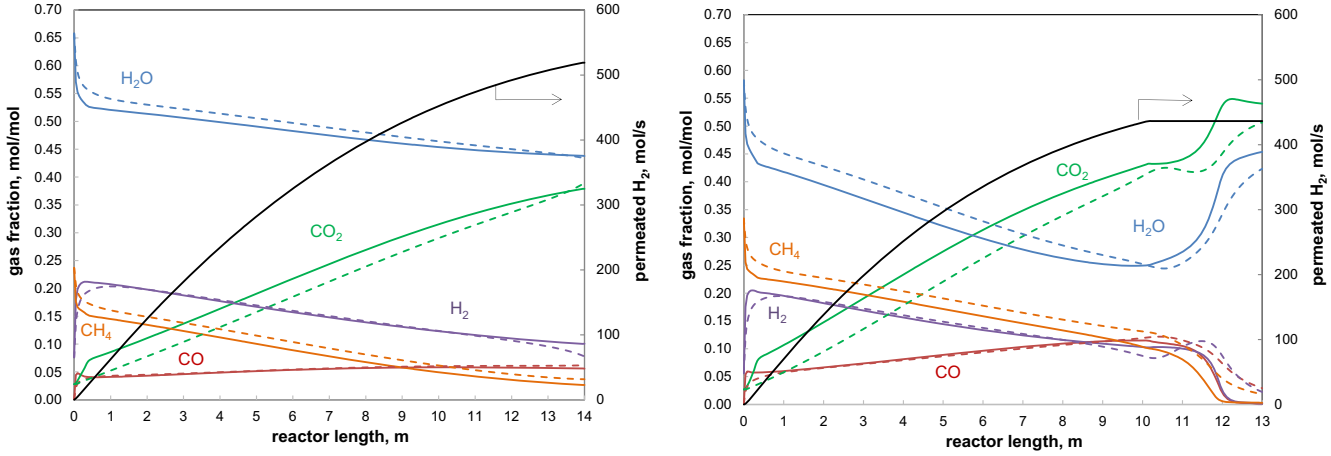

Fig. 9. FBMR (left) and MA-CLR (right) operated at 50 bar 700 °C profiles for the selected geometry. The dashed lines are referred to the bubble phase, while the solid ones refer to the emulsion phase.

Table 7
Detailed energy streams and performance comparison of the different plants.

CO_2 capture technologies $T_{ref}/p_{ref}/SC/p_{perm}$		SMR N/A 890/32/2.7/-	SMR CA-MDEA 890/32/4/-	FBMR Crio 700/50/2.7/4	MA-CLR 700-50-4 H_2O cond 700/50/1.75/4	MA-CLR 650-32-1 H_2O cond 650/32/1.75/1
NG flow rate	kg/s	2.62	2.81	2.62	2.62	2.62
NG thermal Input	$MW_{LHV,\ NG}$	121.94	130.79	121.94	121.94	121.94
Steam-to-carbon ratio		2.7	4	2.7	1.75	1.75
H_2 mass flow rate	kg/s	0.75	0.75	0.85	0.92	0.92
Electricity prod/cons						
Air compressor-Air/exh Fan	MW_{el}	−0.68	−0.91	−0.54	−5.32	−5.51
Gas turbine	MW_{el}	–	–	–	4.73	3.91
H_2, compressors	MW_{el}	−2.27	−2.28	−6.62	−6.75	−9.16
CO_2 compressors	MW_{el}		−2.23	−0.68	−0.33	−0.59
Steam turbine	MW_{el}	3.27	3.79	–	–	–
Pumps	MW_{el}	−0.21	−0.29	−0.07	−0.04	−0.03
Other auxiliaries	MW_{el}	−0.05	−0.15	−0.07	−0.08	−0.10
Net electric power	MW_{el}	0.07	−2.07	−7.98	−7.80	−11.48
Steam export (160 °C, 6 bar)	kg/s	4.02	0.27	0.76	0.66	0.48
H_2 production efficiency η_{H2}	$H_{2,LHV}/NG_{LHV}$	0.74	0.69	0.84	0.90	0.91
Equivalent NG input $m_{NG.eq}$	kg/s	2.41	2.88	2.88	2.88	3.02
H_2 yield	$mol_{H2}/mol_{eq,CH4}$	2.49	2.48	2.79	3.00	3.02
Eq. H_2 production efficiency $\eta_{H2,eq}$	$H_{2,LHV}/NG_{eq.\ LHV}$	0.81	0.67	0.76	0.82	0.79
Heat rate	$Gcal/kNm^3_{H2}$	3.24	3.79	3.24	3.02	3.09
CO_2 specific emissions, E_{CO2}	kg_{CO2}/Nm^3_{H2}	0.82	0.14	0.14	0.00	0.00
Eq. CO_2 spec. em., $E_{CO2,eq}$	kg_{CO2}/Nm^3_{H2}	0.76	0.16	0.21	0.07	0.10
Eq. CO_2 spec. em., $E_{CO2,eq}$	g_{CO2}/MJ_{H2}	70.97	14.55	20.08	6.14	9.57
Equivalent CO_2 avoided	%	–	79%	72%	91%	87%

the FBMR to further enrich the retentate of CO_2. This would allow increasing the CO_2 recovery rate of the CO_2 purification unit, thereby reducing the overall E_{CO2} to 26 $kg_{CO2}/MWh_{H2,LHV}$ and increasing the CO_2 avoidance from 72% to 80%, without any relevant change in the thermal balance of the plant.

For the MA-CLR the η_{H2} is above 90% because the amount of air used in the air reactor is the amount required to provide the stoichiometric O_2 (no excess is required in this case) and therefore less sensible heat is released through the gases. Moreover, a complete fuel oxidation is achieved at the retentate side, which increases the thermal input to the reforming reaction increasing the amount of H_2 produced. In terms of electricity demand, the air compressor consumption is only partly compensated by the gas expander production. However, the H_2 compressors are the most significant consumers of electricity. Similarly to the FBMR plant, the heat for the production of steam-to-export is significantly lower when compared to the conventional plant without capture, because waste heat is mostly available at low temperature and the steam produced is mostly consumed by the process itself. The direct CO_2 emissions from the plant (E_{CO2}) are zero because all the CO_2 is condensed and sent to the final storage. However, the CO_2 avoidance is between 87 and 91% due to the emissions associated to the electricity demand.

The electricity consumption associated with H_2 compression significantly affects the membrane-based plants both from a technical and environmental point of view. The use of sweep gas (in this case only H_2O can be used) would be beneficial to increase the pressure at the permeate side. However, the low amount of heat available for steam generation makes the sweep gas solution less practical as a stand-alone unit, unless steam can be imported from other unit or externally produced with a conventional boiler.

3.6. Cost assessment

The results of the economic analysis are presented in Table 8. The BEC has been listed for the main group of components. For the conventional SMR the largest cost is associated to the reactor (in particular the reformer unit) and the heat exchanger that is used to cool down the exhaust gas from the furnace. The cost of the PSA, which is operated with a high volumetric flow rate, is also above 20% of the BEC. In case CO_2 capture is carried out with a MDEA unit the investment cost increases by about 1/3 mostly due to the cost of CO_2, separation (absorption columns and CO_2 compressors). The cost of the reactors in the FBMR is comparable with the cost required for the reactors in conventional H_2 plants. The cost of H_2 Pd-based membranes accounts for only 5% of the total BEC. The most expensive unit of the plant is represented by the convective heat exchangers network (HEN) for the H_2 and air cooling: due to the low heat transfer coefficient (assumed 35 $W\,m^{-2}\,K^{-1}$ because of the low pressure) and the high volumetric flow rate (especially when H_2 is cooled), the resulting heat transfer area is very high with associated high cost (43% of the BEC). In case of MA-CLR, the highest cost is associated to the CLR reactor units, especially the fuel reactor (ranging from 51% to 57% of the total reactors costs). The cost of the membranes is higher than in the case of FBMR with a slightly higher impact on the BEC. Although the amount of H_2 separated in the MA-CLR membranes is lower compared to the FBMR, the required membrane area is slightly higher. Two main reasons explain this difference: (i) the conversion of CH_4 in the FBMR is higher in the bottom part of the reactor and therefore the $p_{H2,ret}$ is always higher along the reactor than in the case of MA-CLR; (ii) in case of FBMR, part of the H_2 required to supply the heat of reaction is separated with air used as sweep gas which consumes instantaneously the permeated H_2 and therefore the $p_{H2,per}$ is virtually zero. The differences in the reactor geometry for the MA-CLR are dictated by the operating pressure at the retentate/permeate side of the membrane which influence the hydrodynamics of the reactor and the H_2 permeation.

According to the thermodynamic and the economic assessment, the variable costs are higher than the fixed costs. This is particularly pronounced for the case of SMR + CA-MDEA unit due to the low efficiency that leads to high fuel cost. As already anticipated in the previous part of the paper, the energy and economic cost for the electricity-to-import in the membrane reactor plants

Table 8
Detailed comparison of the economics of the selected plants.

CO_2 capture technologies		SMR	SMR	FBMR	MA-CLR 700-50-4	MA-CLR 650-32-1
		N/A	CA-MDEA	Cryo	H_2O cond	H_2O cond
$T_{ref}/p_{ref}/SC/p_{perm}$		890/32/2.7/–	890/32/4/–	700/50/2.7/4	700/50/1.75/4	650/32/1.75/1
Membrane reactor geometry						
FR diameter, m				3.5	2.9	3
FR length, m				14	13	9
Membrane length, m				14	10.2	6
Number of membranes[a]				117	165	350
Economics						
Bare Erected Cost	M€ (% of tot BEC)					
Reactors		10.56 (27.3%)	11.11 (18.7%)	11.06 (27.23%)	15.47(43.71%)	11.35 (33.8%)
Convective cooling HEX		10.67 (27.6%)	13.27 (22.35%)	17.45 (42.96%)	6.50 (18.38%)	6.45 (19.2%)
Turbomachines		3.42 (8.8%)	3.7 (6.3%)	0.25 (0.62%)	1.75 (4.94%)	1.69 (5.02%)
H_2 compressors		1.46 (3.8%)	1.38 (2.3%)	3.51 (8.65%)	3.63 (10.24%)	5.03 (14.98%)
syngas coolers & heat rejection		4.17 (10.8%)	6.58 (11.1%)	4.98 (12.25%)	5.14 (14.52%)	5.24 (15.6%)
PSA unit		8.45 (21.8%)	5.9 (10.0%)	–	–	–
MDEA unit			14.29 (24.1%)	–	–	–
CO_2 compressors			3.12 (5.2%)	1.34 (3.29%)	0.82 (2.31%)	1.21 (3.62%)
H_2 membranes				2.04 (5.01%)	2.09 (5.91%)	2.61 (7.77%)
Total Overnight Cost × CCF	M€/y	14.15	21.70	14.84	12.93	12.27
O&M fixed (others)	M€/y	6.60	9.75	7.95	7.43	7.33
O&M variable (based on 90% plant availability)	M€/y					
Water (process + cooling)		0.63	0.82	0.57	0.36	0.36
Natural gas		31.67	33.97	31.67	31.67	31.68
Steam export		−1.37	−0.09	−0.26	−1.02	−0.16
Electricity		−0.02	1.14	4.81	4.69	6.91
H_2 mass flow rate	kg/s	0.75	0.75	0.85	0.92	0.92
Cost of Hydrogen (COH)	€/Nm^3_{H2}	0.216	0.282	0.220	0.192	0.199
$COH_{variable\ cost}$		0.129	0.150	0.136	0.122	0.132
$COH_{fixed\ cost}$		0.087	0.132	0.084	0.070	0.067
cost of CO_2 avoided	€/t_{CO2}		96.45	6.40	−28.11	−20.10
Cost of CO_2 avoided equiv emiss.	€/$t_{CO2,\ eq}$		109.78	7.98	−33.36	−25.18

[a] Based on a membrane diameter equal to 5 cm.

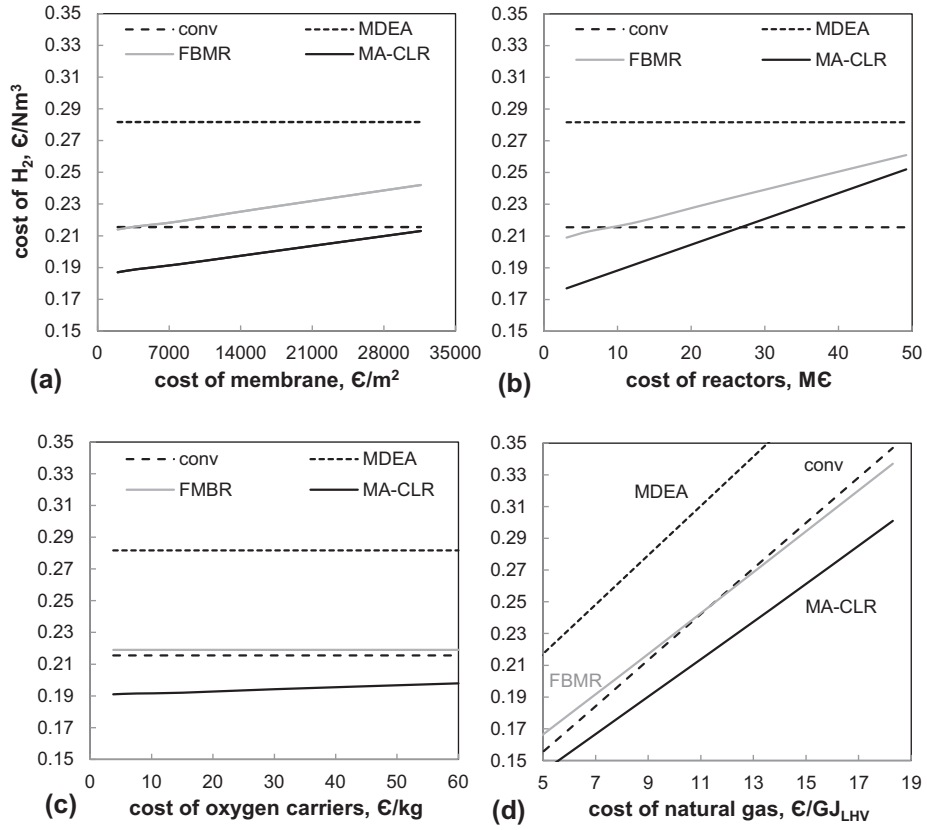

Fig. 10. Sensitivity analysis of the COH using different specific costs for the membrane (a), the reactor (b), the oxygen carriers (c) and the NG (d).

significantly contribute to the COH, which indicates that one of the solutions to improve the plant performance is to separate the H_2 at higher pressure, possibly increasing the reforming pressure.

In terms of overall economic performance, compared to the conventional plant without CO_2 capture, the SMR with chemical absorption has a cost of CO_2 avoided of 83 €/t_{CO2}, while for FBMR the cost of CO_2 avoided is around 6 €/t_{CO2} and it becomes even negative for the MA-CLR due to the reduced operating costs associated with the high efficiencies of the plant. For the MA-CLR, the results show that an investment in R&D for the scale-up and commercialization of the technology would already be beneficial at this stage due to the lower COH compared to the other technologies including the conventional H_2 production plant.

3.7. Sensitivity analysis

A sensitivity analysis has been carried out on the COH by varying the main parameters affecting the COH and the results are presented in Fig. 10. This analysis is required, mainly due to the uncertainties associated on the cost of membranes, of reactors vessels, of the oxygen carrier and on the cost of NG. Since the cost for the membranes accounts for 5–8% (as showed in Table 8), an increase in the cost of Pd membranes up to 4 times the one considered in this work increases the COH up to approximately 0.24 and 0.21 €/m^2 for the FBMR and MA-CLR (@50 bar/700 °C) respectively, but H_2 production with MA-CLR still compares favorably with the state-of-the-art technology without CO_2 capture. In case the cost of the reactor vessels increases by more than twice, the membrane-based plant would cost more than the conventional steam reforming plant. The effect of the cost of the oxygen carrier on the COH is negligible. Finally, in case the cost of NG increases from 0.5 to 2 times the cost used as reference scenario, the COH increases more for the conventional and CA-MDEA plants due to the lower efficiencies of H_2 production. It must be noted that in this analysis it is not considered how the cost of NG would influence the cost of electricity: as the membrane plants require a high electricity import due to the H_2 compressors, an increase in the electricity cost would also increase the COH. For all the sensitivity analyses presented here, the membrane based plants are always more convenient than the plant with conventional CO_2 capture technology by chemical absorption.

4. Conclusions

Two membrane based plants, FBMR and MA-CLR, for the production of H_2 with CO_2 capture using natural gas as feedstock have been studied and compared with reference technologies from a techno-economic point of view. In order to improve the efficiency of the system a lower S/C ratio and higher operating pressures are beneficial for both systems. The reactors temperature affects the heat recovery significantly and the optimal value depends on the specific plant considered. For the membrane based plants the cost of H_2 compression is the most relevant energy cost due to the relatively low H_2 pressure at the permeate side. The membrane reactor can improve the gas conversion and reduce the number of components required in the plant. In case of FBMR, the cost of the HEN is drastically limiting the economic performance of the plant, while for the case of MA-CLR the design of an interconnected fluidized bed reactor operated at high pressure needs to be experimentally demonstrated. The COH associated to the FBMR is only slightly higher than the conventional system without CO_2 capture and the cost of CO_2 avoided is about 6 €/t_{CO2}, while for the MA-CLR the economic advantages are evident in terms of reforming efficiencies, CCR and COH.

Acknowledgements

The authors are grateful to NWO/STW for the financial support through the VIDI project ClingCO_2-project number 12365.

References

[1] Wawrzinek K, Keller C. Industrial hydrogen production & technology. FuncHy-Workshop; 2007. http://www.hzg.de/imperia/md/content/gkss/institut_fuer_werkstoffforschung/wtn/h2-speicher/funchy/funchy-2007/5_linde_wawrzinek_funchy-2007.pdf.
[2] Dunn S. Hydrogen futures: toward a sustainable energy system. Int J Hydrogen Energy 2002;27:235–64.
[3] Aasberg-Petersen K, Bak Hansen JH, Christensen TS, Dybkjaer I, Christensen PS, Stub Nielsen C, et al. Technologies for large-scale gas conversion. Appl Catal A Gen 2001;221:379–87.
[4] Foster Wheeler. Steam-hydrocarbon reformer furnace design n.d.:1–26. http://www.fosterwheeler.fi/getmedia/3f65b6f5-ab13-4f8f-91fe-782e097ccdfc/Steam-Hydrocarbon-Reformer-Furnace-Design.pdf.aspx.
[5] Rostrup-Nielsen JR. Production of synthesis gas. Catal Today 1993;18:305–24.
[6] Rostrup-Nielsen J. New aspects of syngas production and use. Catal Today 2000;63:159–64.
[7] Meerman JC, Hamborg ES, van Keulen T, Ramírez A, Turkenburg WC, Faaij a PC. Techno-economic assessment of CO_2 capture at steam methane reforming facilities using commercially available technology. Int J Greenhouse Gas Control 2012;9:160–71.
[8] Collodi G. Hydrogen production via steam reforming with CO_2 capture. Chem Eng Trans 2010;19:37–42. Available from: <http://www.aidic.it/CISAP4/webpapers/7Collodi.pdf>.
[9] Carrara A, Perdichizzi A, Barigozzi G. Simulation of an hydrogen production steam reforming industrial plant for energetic performance prediction. Int J Hydrogen Energy 2010;35:3499–508.
[10] Martínez I, Romano MC, Chiesa P, Grasa G, Murillo R. Hydrogen production through sorption enhanced steam reforming of natural gas: thermodynamic plant assessment. Int J Hydrogen Energy 2013;38:15180–99.
[11] DOE/NETL. Assessment of hydrogen production with CO_2 capture volume 1: baseline state-of- the-art plants; 2010. https://www.netl.doe.gov/File%20Library/research/energy%20analysis/publications/H2_Prod_Vol1_2010.pdf.
[12] Barba D, Giacobbe F, De Cesaris A, Farace A, Iaquaniello G, Pipino A. Membrane reforming in converting natural gas (part one). Int J Hydrogen Energy 2008;33:3700–9.
[13] Dittmar B, Behrens A, Schödel N, Rüttinger M, Franco T, Straczewski G, et al. Methane steam reforming operation and thermal stability of new porous metal supported tubular palladium composite membranes. Int J Hydrogen Energy 2013;38:8759–71.
[14] Gallucci F, Annaland M, Kuipers J. Autothermal reforming of methane with integrated CO_2 capture in a novel fluidized bed membrane reactor. Part 1: experimental demonstration. Top Catal 2008;51:133–45.
[15] Gallucci F, van Sint Annaland M, Kuipers J. Autothermal reforming of methane with integrated CO_2 capture in a novel fluidized bed membrane reactor. Part 2 comparison of reactor configurations. Top Catal 2008;51:146–57.
[16] Roses L, Gallucci F, Manzolini G, van Sint Annaland M. Experimental study of steam methane reforming in a Pd-based fluidized bed membrane reactor. Chem Eng J 2013;222:307–20.
[17] Sircar S, Waldron W, Rao M, Anand M. Hydrogen production by hybrid SMR–PSA–SSF membrane system. Sep Purif Technol 1999;17:11–20.
[18] Boon J, Pieterse JAZ, Dijkstra JW, Van Delft YC, Veenstra P, Jansen D. Benchmarking of hydrogen selective membranes: experimental and modelling approach to compare membrane performance. Energy Procedia 2013;37:1020–9.
[19] Fernandez E, Coenen K, Helmi A, Melendez J, Zuñiga J, Pacheco Tanaka DA, et al. Preparation and characterization of thin-film Pd–Ag supported membranes for high-temperature applications. Int J Hydrogen Energy 2015.
[20] Gallucci F, Fernandez E, Corengia P, van Sint Annaland M. Recent advances on membranes and membrane reactors for hydrogen production. Chem Eng Sci 2013;92:40–66.
[21] Michelsen FA, Wilhelmsen Ø, Zhao L, Åsen KI. A distributed dynamic model of a monolith hydrogen membrane reactor. Energy Convers Manage 2013;67:160–70.
[22] De Falco M, Iaquaniello G, Marelli L. Reformer and membrane modules plant for natural gas conversion hydrogen: performance assessment. In: 9th international conference chemical process engineering ICheaP-9. p. 1407–12.
[23] Iaquaniello G, Giacobbe F, Morico B, Cosenza S, Farace A. Membrane reforming in converting natural gas to hydrogen: production costs, Part II. Int J Hydrogen Energy 2008;33:6595–601.
[24] Manzolini G, Dijkstra JW, Macchi E, Jansen D. Technical economic evaluation of a system for electricity production CO_2 capture using membrane reformer with permeate side combustion. In: ASME Turbo Expo 2006, Barcelona. p. 1–11.
[25] Johannessen E, Jordal K. Study of a H_2 separating membrane reactor for methane steam reforming at conditions relevant for power processes with CO_2 capture. Energy Convers Manage 2005;46:1059–71.
[26] Jordal K, Bredesen R, Kvamsdal HM, Bolland O. Integration of H_2-separating membrane technology in gas turbine processes for CO_2 capture. Energy 2004;29:1269–78.

[27] Atsonios K, Panopoulos KD, Doukelis A, Koumanakos A, Kakaras E. Exergy analysis of a hydrogen fired combined cycle with natural gas reforming and membrane assisted shift reactors for CO_2 capture. Energy Convers Manage 2012;60:196–203.
[28] Chiesa P, Romano MC, Spallina V, Turi DM, Mancuso L. Efficient low CO_2 emissions power generation by mixed conducting membranes. Energy Procedia 2013;37:905–13.
[29] Adanez J, Abad A, Garcia-Labiano F, Gayan P, de Diego L. Progress in chemical-looping combustion and reforming technologies. Prog Energy Combust Sci 2012;38:215–82.
[30] Ortiz M, de Diego LF, Abad A, García-Labiano F, Gayán P, Adánez J. Hydrogen production by auto-thermal chemical-looping reforming in a pressurized fluidized bed reactor using Ni-based oxygen carriers. Int J Hydrogen Energy 2010;35:151–60.
[31] de Diego LF, Ortiz M, García-Labiano F, Adánez J, Abad A, Gayán P. Hydrogen production by chemical-looping reforming in a circulating fluidized bed reactor using Ni-based oxygen carriers. J Power Sources 2009;192:27–34.
[32] Tang M, Xu L, Fan M. Progress in oxygen carrier development of methane-based chemical-looping reforming: a review. Appl Energy 2015;151:143–56.
[33] Ryden M, Lyngfelt A. Using steam reforming to produce hydrogen with carbon dioxide capture by chemical-looping combustion. Int J Hydrogen Energy 2006;31:1271–83.
[34] Dybkjær I. Synthesis gas technology. Hydrocarb Eng 2006;11:33–6.
[35] Haussinger P, Lohmuller R, Watson AM. Hydrogen, 2. Production. In: Wiley, editor. Ullman's Encycl Ind Chem; 2012. p. 249–98.
[36] Farshchi Tabrizi F, Mousavi SAHS, Atashi H. Thermodynamic analysis of steam reforming of methane with statistical approaches. Energy Convers Manage 2015;103:1065–77.
[37] Yang X, Da J, Yu H, Wang H. Characterization and performance evaluation of Ni-based catalysts with Ce promoter for methane and hydrocarbons steam reforming process. Fuel 2016;179:353–61.
[38] Alstom Power Energy Recovery. Gas cooling systems for steam reforming plants.
[39] Fernandez E, Helmi A, Coenen K, Melendez J, Viviente JL, Pacheco Tanaka DA, et al. Development of thin Pd–Ag supported membranes for fluidized bed membrane reactors including WGS related gases. Int J Hydrogen Energy 2015;40:3506–19.
[40] Roghair I, Gallucci F, van Sint Annaland M. Modeling and simulation of heterogeneous catalytic processes. Elsevier; 2014.
[41] Li H, Hu Y, Ditaranto M, Willson D, Yan J. Optimization of cryogenic CO_2 purification for oxy-coal combustion. Energy Procedia 2013;37:1341–7.
[42] Besong MT, Maroto-Valer MM, Finn AJ. Study of design parameters affecting the performance of CO_2 purification units in oxy-fuel combustion. Int J Greenhouse Gas Control 2013;12:441–9.
[43] Chiesa P, Campanari S, Manzolini G. CO_2 cryogenic separation from combined cycles integrated with molten carbonate fuel cells. Int J Hydrogen Energy 2011;36:10355–65.
[44] Medrano JA, Spallina V, van Sint Annaland M, Gallucci F. Thermodynamic analysis of a membrane-assisted chemical looping reforming reactor concept for combined H_2 production and CO_2 capture. Int J Hydrogen Energy 2014;39:4725–38.
[45] Medrano JA, Hamers HP, Williams G, van Sint Annaland M, Gallucci F. NiO/$CaAl_2O_4$ as active oxygen carrier for low temperature chemical looping applications. Appl Energy 2015;158:86–96.
[46] Cho P, Mattisson T, Lyngfelt A. Carbon formation on nickel and iron oxide-containing oxygen carriers for chemical-looping combustion. Ind Eng Chem Res 2005;44:668–76.
[47] EBTF. European best practice guidelines for assessment of CO_2 capture technologies; 2011.
[48] Peters MS, Timmerhaus KD. Plant design and economics for chemical engineers. 4th ed, 1991.
[49] Turton R, Bailie RC, Whiting WB, Shaeiwitz JA, Bhattacharyya D. Economic analysis of chemical processes. In: Analysis synthesis and design chemical processes. Prentice Hall; 2012.
[50] Pall corporation. High-performance, durable, palladium alloy membrane for hydrogen separation and purification; 2009. https://www.hydrogen.energy.gov/pdfs/review11/pd005_damle_2011_p.pdf.
[51] Manzolini G, Macchi E, Gazzani M. CO_2 capture in natural gas combined cycle with SEWGS. Part B: Economic assessment. Int J Greenhouse Gas Control 2013;12:502–9.
[52] Manzolini G, Dijkstra JW, Macchi E, Jansen D. Technical economic evaluation of a system for electricity production with CO_2 capture using a membrane reformer with permeate side combustion. Conference proceeding ASME turbo EXPO 2006:1–11.
[53] Baasel WD. Preliminary chemical engineering plant design. New York: Van Nostrand Reinhold; 1989.
[54] Campanari S, Chiesa P, Manzolini G, Bedogni S. Economic analysis of CO_2 capture from natural gas combined cycles using molten carbonate fuel cells. Appl Energy 2014;130:562–73.
[55] NREL. Equipment design and cost estimation for small modular biomass systems, synthesis gas cleanup, and oxygen separation equipment. San Francisco; 2006. http://www.nrel.gov/docs/fy06osti/39943.pdf.
[56] Rubin E, Booras G, Davison J, Ekstrom C, Matuszewski M, McCoy S, et al. Toward a common method of cost estimation for CO_2 capture and storage at fossil fuel power plants.; 2013. http://www.cmu.edu/epp/iecm/rubin/PDFfiles/2012/CCS Task Force_White Paper_FINAL_Jan 15 2013.pdf.
[57] Gerdes K, Summers WM, Wimer J. Cost Estimation Methodology for NETL assessments of power plant performance. Pittsburgh; 2011. https://www.netl.doe.gov/File%20Library/research/energy%20analysis/publications/QGESSNETLCostEstMethod.pdf.
[58] Spallina V, Battistella A, Medrano JA, Campos Velarde I, Gallucci F, van Sint Annaland M. Design and modelling of novel membrane-assisted reactor concept for H_2 production with near zero CO_2 emissions. World Hydrogen Technology Conversion 2015, Sydney; 2015.
[59] Kunii D, Levenspiel O. The K-L reactor model for circulating fluidized beds. Chem Eng Sci 2000;55:4563–70.
[60] Kunii D, Levenspiel O. Bubbling bed model. Ind Eng Chem Res 1968;7:446–52.
[61] Levenspiel O. G/S reactor models—packed beds, bubbling fluidized beds, turbulent fluidized beds and circulating (fast) fluidized beds. Powder Technol 2002;122:1–9.
[62] Iliuta I, Tahoces R, Patience GS, Rifflart S, Luck F. Chemical-looping combustion process: kinetics and mathematical modeling. AIChE J 2010;56:1063–79.
[63] Medrano JA, Fernandez E, Melendez J, Parco M, Alfredo D, Tanaka P, et al. Pd-based metallic supported membranes: high- temperature stability and fluidized bed reactor testing. Int J Hydrogen Energy 2015 [In press].
[64] Fernandez E, Medrano JA, Melendez J, Parco M, van Sint Annaland M, Gallucci F, et al. Preparation and characterization of metallic supported thin Pd–Ag membranes for high temperature hydrogen separation. Chem Eng J 2015 [In press].
[65] Peters Max S, Timmerhaus Klaus D. Plant design and economics for chemical engineers. 4th ed. McGraw-Hill; 1991.